International Journal of Solids and Structures 46 (2009) 938–951

Contents lists available at ScienceDirect

International Journal of Solids and Structures

journal homepage: www.elsevier.com/locate/ijsolstr

A domain integral for the calculation of generalized stress intensity factors in sliding complete contacts

E. Giner *, M. Tur, F.J. Fuenmayor

Departamento de Ingeniería Mecánica y de Materiales, Centro de Investigación de Tecnología de Vehículos (CITV), Universidad Politécnica de Valencia, Camino de Vera, 46022 Valencia, Spain

ARTICLE INFO

Article history:
Received 1 August 2008
Received in revised form 27 September 2008
Available online 17 October 2008

Keywords:
Generalized stress intensity factor
Sliding frictional contact
Fretting fatigue
Domain integral
Finite element method

ABSTRACT

In this study, a procedure for calculating the generalized stress intensity factor (GSIF) for 2D sliding complete contacts is presented. The method is based on a domain integral equivalent to a path-independent integral. The domain character of the approach makes it very suitable for the post-processing of finite element solutions. The robustness and accuracy of the method are assessed through numerical examples, comparing the obtained results with other techniques, such as stress extrapolation and the path-independent contour integral. In addition, the multiplier constants for other terms in the expansion series are also computed.

1. Introduction

Mechanical components with abrupt changes in geometry often lead to theoretical singularities in the strain and stress fields (assuming linear elastic behaviour). This situation arises in components with re-entrant corners or V-notches, including crack problems of linear elastic fracture mechanics (LEFM) as a particular case, and also in certain complete contacts between solids. A contact is said to be complete when the contact area is independent of the normal load due to an abrupt change in the geometry of one of the contacting bodies.

In this study, we will concentrate on the characterization of singularities that usually exist at the end of complete contact zones under sliding conditions. Examples of real problems that can be modelled with this behaviour are hub-axle joints and spline connections between split shafts. The corresponding fatigue analysis of these components is of great interest and several authors have proposed the study of the crack initiation and propagation stages through the analysis of the stress field in the vicinity of the singular corners (Hattori et al., 1988; Hattori, 1994; Mugadu et al., 2002; Mugadu and Hills, 2002; Hattori et al., 2003).

Assuming a linear elastic behaviour, the stress field at the end of the contact zone can be either singular or non-singular, depending on the geometric configuration, sliding direction, etc. Of course, singular configurations tend to be more critical, justifying a more detailed study and characterization. If we express the stress field as a series expansion, it is usually assumed that the singular term dominates over the other in a region sufficiently close to the contact corner and, hence, the stress field can be described by only this term in this region. This is analogous to a LEFM approach to crack problems. The singular field is characterized by two parameters: the singularity order (related to the eigenvalue λ) and the generalized

* Corresponding author. Tel.: +34 96 3877621; fax: +34 96 3877629.
E-mail address: eginerm@mcm.upv.es (E. Giner).

0020-7683/$ - see front matter © 2008 Elsevier Ltd. All rights reserved.
doi:10.1016/j.ijsolstr.2008.10.007

stress intensity factor K^C (GSIF). The end of the contact zone can exhibit varying contact conditions during load cycles: stick, sliding or opening (although in this latter case the contact is no longer complete). The singularity order can be analytically computed *a priori* and depends on the geometry of the contact bodies, material properties, friction coefficient and sliding direction. For an adhered condition, the problem can be assimilated to a V-notch in a monolithic solid and therefore the asymptotic solution proposed by Williams (1952) is applicable. For a sliding condition, the asymptotic solution was provided by Gdoutos and Theocaris (1975) and Comninou (1976).

The GSIF depends on the boundary conditions of each problem and its value (together with the order of singularity) completely characterizes the stress field within the singularity dominated zone. As a consequence, it is often claimed that the GSIF value is the key parameter that controls the crack nucleation and its eventual propagation (Hattori et al., 1988; Hattori et al., 2003; Mugadu and Hills, 2002), leading to the necessity of its evaluation (analogous approaches have been considered for V-notches, e.g. Lazzarin and Zambardi, 2001). The GSIF calculation is usually performed using numerical methods, such as the finite element method. A stress extrapolation technique can be applied to compute the GSIF, as it is often found in the literature (Hattori, 1994; Hattori et al., 2003). However, the stress extrapolation technique has several disadvantages: firstly, it must be applied within the singularity dominated zone, where the FE solution is much less accurate (for a given mesh) than in regions far from the singular point. Secondly, the selection of the stress collocation points is arbitrary and needs a great deal of user intervention, which can be cumbersome. Using another approach, (Lazzarin et al. (2008)) show that it is possible to infer the notch stress intensity factor (NSIF) through the numerical estimation of the averaged strain energy density (SED). However, they only apply this method to monolithic wedges and not to sliding contact singularities.

In this work, we propose a domain integral method for the calculation of the GSIF in sliding complete contacts. The energy-based character of this approach provides great accuracy when applied to a numerical solution (such as a FE solution) as a post-processing technique. The domain over which the integral is performed can exclude the singularity region (where the numerical error is greatest). Very good GSIF estimations can be obtained without using very refined meshes, higher order elements or specially conceived singular elements that reproduce the singularity (Tur et al., 2002a,b). Moreover, its application is highly systematic and the user intervention is not crucial. Therefore, it has the same advantages than the well-known EDI method (equivalent domain integral to the *J*-contour integral), widely used for the analysis of LEFM problems (Li et al., 1985; deLorenzi, 1985; Banks-Sills, 1991). More recent works by Gosz and Moran (2002), Omer and Yosibash (2005) and Yosibash and Omer (2007) also show that the use domain integrals provides a good means to characterize 3D crack and notch problems.

The domain integral is based on a path-independent contour integral previously proposed by the authors (Fuenmayor et al., 2005; Tur et al., 2006). In principle, the contour integral exhibits similar advantages due to its energy-based character. However, in this work we show that the domain integral yields more accurate results than the contour integral, as it involves more information from the numerical solution in its computation. In addition, it is more robust and easier to implement in a FE code, since the integration over the elements is consistent with the FE formulation. In this study, we derive the domain integral and verify its behaviour with numerical examples. The GSIFs calculated compare favourably to the stress extrapolation and contour integral results. The proposed methodology also enables the computation of the multiplier constants that play the role of the GSIF for other terms in the asymptotic expansion series, as shown in the numerical examples.

2. Path-independent contour integral

In order to introduce the domain integral, and for the sake of completeness, it is necessary to review the energy-based approach that leads to the path-independent contour integral for sliding complete contacts (Fuenmayor et al., 2005; Tur et al., 2006). This contour integral will then be recast as the equivalent domain form. The approach is based on the Betti's reciprocal theorem. This theorem was also used by Stern et al. (1976) for the SIF calculation in LEFM and by Szabó and Babuška (1991) for monolithic V-notches.

Fig. 1 shows a sketch of the problem where two coordinate systems, cartesian and polar, are defined with the origin at the end of the contact zone. A small-displacement assumption is made, together with a linear elastic material behaviour. Both solids are considered to be infinite half-spaces, being solid (1) the body that contacts onto the solid (2) under sliding friction conditions.

Assuming no body forces and no initial strains, the Betti's reciprocal theorem applied to one solid (i) establishes that

$$\oint_{(i)} (\sigma_{jk}^{(i)} \bar{u}_k^{(i)} - \bar{\sigma}_{jk}^{(i)} u_k^{(i)}) n_j \mathrm{d}s = 0 \tag{1}$$

where $u^{(i)}$, $\bar{u}^{(i)}$ are two displacement fields that satisfy the equilibrium equations. The stress fields $\sigma^{(i)}$, $\bar{\sigma}^{(i)}$ correspond to the displacement fields $u^{(i)}$ and $\bar{u}^{(i)}$, respectively. Combining the application of Betti's reciprocal theorem to both solids, the following equation holds

$$\oint_{(1)} (\sigma_{jk}^{(1)} \bar{u}_k^{(1)} - \bar{\sigma}_{jk}^{(1)} u_k^{(1)}) n_j \mathrm{d}s + \oint_{(2)} (\sigma_{jk}^{(2)} \bar{u}_k^{(2)} - \bar{\sigma}_{jk}^{(2)} u_k^{(2)}) n_j \mathrm{d}s = 0 \tag{2}$$

where the closed contours (1) and (2) used to calculate the integrals are shown in Fig. 2.

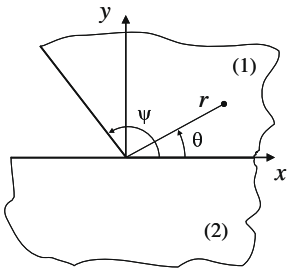

Fig. 1. Bodies sliding with friction in a complete contact.

Assuming that there are no tractions acting on the free boundaries of the solids and that the stress field $\bar{\sigma}^{(i)}$ fulfils this boundary condition, the following path independent integral I_{Γ^*} can be defined from Eq. (2):

$$I_{\Gamma^*} = \int_{\Gamma^*} (\sigma_{jk}\bar{u}_k - \bar{\sigma}_{jk}u_k)n_j \mathrm{d}s + \int_{\Gamma_C^{*(1)}} (\sigma_{jk}^{(1)}\bar{u}_k^{(1)} - \bar{\sigma}_{jk}^{(1)}u_k^{(1)})n_j \mathrm{d}s - \int_{\Gamma_C^{*(2)}} (\sigma_{jk}^{(2)}\bar{u}_k^{(2)} - \bar{\sigma}_{jk}^{(2)}u_k^{(2)})n_j \mathrm{d}s \tag{3}$$

It is easy to show that Eq. (3) is path-independent starting from (2) and rearranging some of the terms according to the paths defined in Fig. 2. A detailed proof is given in Fuenmayor et al. (2005), Tur et al. (2006). The integration paths used in (3) are shown in Fig. 3. Γ^* is an arbitrary path from the free surface of solid (2) to the free surface of solid (1). This line surrounds the singular point. The paths $\Gamma_C^{*(i)}$ are also involved in (3) defined along the contact line for each of the solids. These paths $\Gamma_C^{*(i)}$ start from the singular point up to the intersection with Γ^*. Obviously, the displacement and stress fields in the first integral of (3) refer to the corresponding solid, depending on the portion of the path Γ^* that is to be integrated.

3. Singular field in sliding complete contacts

The stress field in a region sufficiently close to the end of the contact between a flat indenter and an infinite half-plane was derived by Gdoutos and Theocaris (1975) and Comninou (1976). They carried out an asymptotic analysis for the sliding or adhesion conditions and assuming dissimilar materials for the indenter and for the half-plane. Mugadu et al. (2002) particularized these results in order to analyze complete contacts in fretting fatigue. In this section, we succinctly review the asymptotic solution and introduce the notation that is used. We assume elastically similar bodies, with isotropic and homogeneous material. The reference system is defined in Fig. 1 and ψ is the indenter angle.

The stress fields $\sigma^{(1)}$, $\sigma^{(2)}$ and the displacements $u^{(1)}$, $u^{(2)}$ can be derived from the Airy stress functions $\phi^{(1)}$, $\phi^{(2)}$ and fulfil the boundary conditions for each body, including along the contact conditions. From the Airy stress function, the stress field is

$$\sigma_{rr} = \frac{1}{r}\frac{\partial\phi}{\partial r} + \frac{1}{r^2}\frac{\partial^2\phi}{\partial\theta^2}; \quad \sigma_{\theta\theta} = \frac{\partial^2\phi}{\partial r^2}; \quad \sigma_{r\theta} = -\frac{1}{r}\frac{\partial^2\phi}{\partial r\partial\theta} + \frac{1}{r^2}\frac{\partial\phi}{\partial\theta} \tag{4}$$

and the displacement field is

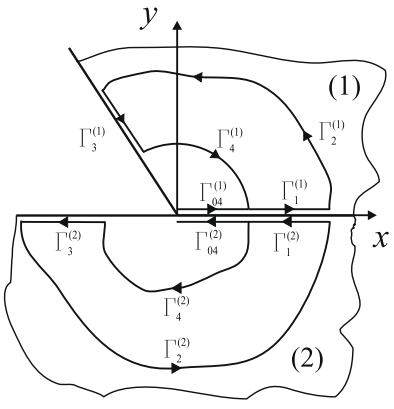

Fig. 2. Closed contours for the application of Betti's reciprocal theorem.

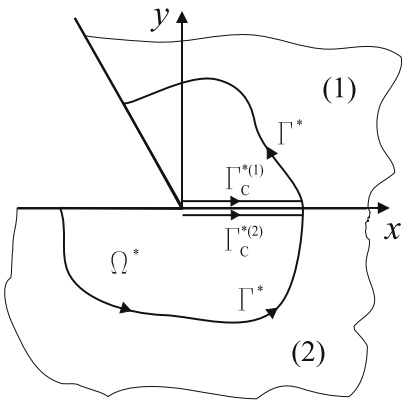

Fig. 3. Integration path Γ^* that surrounds the singular point. The path Γ_C^* is defined along the contact line, from the singular point to the intersection with Γ^*.

$$
\begin{aligned}
2\mu\frac{\partial u_r}{\partial r} &= \frac{1}{r}\frac{\partial \phi}{\partial r}+\frac{1}{r^2}\frac{\partial^2\phi}{\partial\theta^2}-\left(1-\frac{m}{4}\right)\nabla^2\phi \\
\mu\left(\frac{\partial u_\theta}{\partial r}-\frac{u_\theta}{r}+\frac{1}{r}\frac{\partial u_r}{\partial\theta}\right) &= -\frac{1}{r}\frac{\partial^2\phi}{\partial r\partial\theta}+\frac{1}{r^2}\frac{\partial\phi}{\partial\theta}
\end{aligned}
\tag{5}
$$

where the constant m takes the value $m = 4/(1+\nu)$ for plane stress and $m = 4(1-\nu)$ for plane strain, ν is the Poisson's ratio and μ the shear modulus. For each solid (i) the Airy function satisfies the biharmonic equation

$$\nabla^4\phi^{(i)} = 0 \tag{6}$$

The general solution to (6) is of the form

$$\phi^{(i)}(r,\theta) = r^{\lambda+1}(a^{(i)}\mathrm{s}_+\theta + b^{(i)}\mathrm{c}_+\theta + c^{(i)}\mathrm{s}_-\theta + d^{(i)}\mathrm{c}_-\theta) \tag{7}$$

where the parameters $a^{(i)}$, $b^{(i)}$, $c^{(i)}$, $d^{(i)}$ are to be calculated and the following definitions are used $\mathrm{s}_+\theta = \sin(1+\lambda)\theta$, $\mathrm{s}_-\theta = \sin(1-\lambda)\theta$, $\mathrm{c}_+\theta = \cos(1+\lambda)\theta$ and $\mathrm{c}_-\theta = \cos(1-\lambda)\theta$. From Fig. 2, the boundary conditions for the free boundaries can be expressed as

$$\sigma_{\theta\theta}^{(2)}(r,-\pi) = 0; \quad \sigma_{r\theta}^{(2)}(r,-\pi) = 0; \quad \sigma_{\theta\theta}^{(1)}(r,\psi) = 0; \quad \sigma_{r\theta}^{(1)}(r,\psi) = 0 \tag{8}$$

From the continuity of displacements and stresses along the contact line and given the sliding condition with friction, another set of four equations must be satisfied:

$$
\begin{aligned}
&\sigma_{r\theta}^{(2)}(r,0)+f\sigma_{\theta\theta}^{(2)}(r,0) = 0; \quad \sigma_{r\theta}^{(1)}(r,0)+f\sigma_{\theta\theta}^{(1)}(r,0) = 0 \\
&\sigma_{\theta\theta}^{(2)}(r,0)-\sigma_{\theta\theta}^{(1)}(r,0) = 0; \quad u_\theta^{(2)}(r,0)-u_\theta^{(1)}(r,0) = 0
\end{aligned}
\tag{9}
$$

where the parameter f is the friction coefficient. For a sliding of the indenter in the positive direction of the x axis, we define $f > 0$, whereas $f < 0$ if the indenter slides in the opposite sense. By applying the Mellin transform (Mugadu et al., 2002; Barber, 2002) to the set of conditions given by (8) and (9) and considering the Eqs. 4, 5 and 7, the following system with eight unknowns can be formulated:

$$
\begin{bmatrix} [A_{11}] & [A_{12}] \\ [A_{21}] & [A_{22}] \end{bmatrix}
\begin{Bmatrix} v^{(1)} \\ v^{(2)} \end{Bmatrix} =
\begin{Bmatrix} \{0\} \\ \{0\} \end{Bmatrix}
\tag{10}
$$

where $v^{(i)} = (a^{(i)}b^{(i)}c^{(i)}d^{(i)})^{\mathrm{T}}$. The same result can be obtained using the Michell solution for the polar components of displacement (Barber, 2002). The submatrices $[A_{ij}]$ are

$$
[A_{11}] = \begin{bmatrix}
(\lambda+1)\cos(\lambda\pi) & (\lambda+1)\sin(\lambda\pi) & (1-\lambda)\cos(\lambda\pi) & (\lambda-1)\sin(\lambda\pi) \\
\sin(\lambda\pi) & -\cos(\lambda\pi) & -\sin(\lambda\pi) & -\cos(\lambda\pi) \\
0 & 0 & 0 & 0 \\
0 & 0 & 0 & 0
\end{bmatrix}
\tag{11}
$$

$$[A_{12}] = \begin{bmatrix} 0 & 0 & 0 & 0 \\ 0 & 0 & 0 & 0 \\ (\lambda+1)\mathrm{c}_+\psi & -(\lambda+1)\mathrm{s}_+\psi & (1-\lambda)\mathrm{c}_-\psi & -(1-\lambda)\mathrm{s}_-\psi \\ \mathrm{s}_+\psi & \mathrm{c}_+\psi & \mathrm{s}_-\psi & \mathrm{c}_-\psi \end{bmatrix} \tag{12}$$

$$[A_{21}] = \begin{bmatrix} -(\lambda+1) & f(\lambda+1) & (\lambda-1) & f(\lambda+1) \\ 0 & 0 & 0 & 0 \\ 0 & 1 & 0 & 1 \\ (\lambda+1) & 0 & (1-\lambda-m) & 0 \end{bmatrix} \tag{13}$$

$$[A_{22}] = \begin{bmatrix} 0 & 0 & 0 & 0 \\ -(\lambda+1) & f(\lambda+1) & (\lambda-1) & f(\lambda+1) \\ 0 & -1 & 0 & -1 \\ -(\lambda+1) & 0 & -(1-\lambda-m) & 0 \end{bmatrix} \tag{14}$$

The system of Eq. (10) has a nontrivial solution if the matrix determinant is zero. Computing the determinant and after algebraic manipulation, the following characteristic equation is obtained:

$$\Delta(\lambda) = \cos(\lambda\pi)(\sin^2\lambda\psi - \lambda^2\sin^2\psi) + 0.5\sin(\lambda\pi)(\sin 2\lambda\psi + \lambda\sin 2\psi) + f\lambda(1+\lambda)\sin(\lambda\pi)\sin^2\psi = 0 \tag{15}$$

The factor $4m(\lambda+1)\sin(\lambda+1)\pi$ in $\Delta(\lambda)$ is omitted when searching for the roots of the characteristic Eq. (15), since the roots of the factor ($\lambda=-1$ and the rest of integers) have no physical meaning. The roots of (15) are the eigenvalues λ_j ($j=1,\ldots,\infty$). The eigenvector corresponding to a given eigenvalue λ_j is computed by substitution of the eigenvalue in (10) and solving the indeterminate system as a function of a constant K^C and expressing the parameters $a_j^{(i)}$, $b_j^{(i)}$, $c_j^{(i)}$, $d_j^{(i)}$ in terms of this constant. Once these parameters are obtained, the displacement field can be expressed as

$$\{u^{(i)}(r,\theta)\} = \begin{Bmatrix} u_r^{(i)} \\ u_\theta^{(i)} \end{Bmatrix} = \sum_{j=1}^{\infty} K_j^C r^{\lambda_j}\{\Psi_j^{(i)}(\theta,\lambda_j)\} \tag{16}$$

where

$$\{\Psi_j^{(i)}(\theta,\lambda_j)\} = \frac{1}{2\mu}\begin{Bmatrix} -(\lambda_j+1)(a_j^{(i)}\mathrm{s}_+\theta + b_j^{(i)}\mathrm{c}_+\theta) + (m-1-\lambda_j)(c_j^{(i)}\mathrm{s}_-\theta + d_j^{(i)}\mathrm{c}_-\theta) \\ (\lambda_j+1)(-a_j^{(i)}\mathrm{c}_+\theta + b_j^{(i)}\mathrm{s}_+\theta) + (\lambda_j-1+m)(c_j^{(i)}\mathrm{c}_-\theta - d_j^{(i)}\mathrm{s}_-\theta) \end{Bmatrix} \tag{17}$$

and the stress field as

$$\{\sigma^{(i)}(r,\theta)\} = \begin{Bmatrix} \sigma_{rr}^{(i)} \\ \sigma_{\theta\theta}^{(i)} \\ \sigma_{r\theta}^{(i)} \end{Bmatrix} = \sum_{j=1}^{\infty} K_j^C r^{\lambda_j-1}\{\Phi_j^{(i)}(\theta,\lambda_j)\} \tag{18}$$

where

$$\{\Phi_j^{(i)}(\theta,\lambda_j)\} = \begin{Bmatrix} \lambda_j(\lambda_j+1)(-a_j^{(i)}\mathrm{s}_+\theta - b_j^{(i)}\mathrm{c}_+\theta) + \lambda_j(\lambda_j-3)(-c_j^{(i)}\mathrm{s}_-\theta - d_j^{(i)}\mathrm{c}_-\theta) \\ \lambda_j(\lambda_j+1)(a_j^{(i)}\mathrm{s}_+\theta + b_j^{(i)}\mathrm{c}_+\theta + c_j^{(i)}\mathrm{s}_-\theta + d_j^{(i)}\mathrm{c}_-\theta) \\ \lambda_j(\lambda_j+1)(-a_j^{(i)}\mathrm{c}_+\theta + b_j^{(i)}\mathrm{s}_+\theta) + \lambda_j(1-\lambda_j)(-c_j^{(i)}\mathrm{c}_-\theta + d_j^{(i)}\mathrm{s}_-\theta) \end{Bmatrix} \tag{19}$$

The corresponding traction vector for a contour whose unit normal vector is n_j is defined as $T_k^{(i)} = \sigma_{jk}^{(i)} n_j$.

4. Extraction field

In this section, we define an auxiliary displacement field (and its corresponding auxiliary stress field) that substituted in Eq. (3) can be used to compute the GSIF K_j^C associated with the j-term of the series expansions (16), (18). This auxiliary field has been specially conceived so as to cancel the integrand of the path integrals along the contact line $\Gamma_C^{*(i)}$ in Eq. (3) and we call it extraction field. This judicious choice of the auxiliary field greatly simplifies the evaluation of the path-independent integrals, since avoids the integration up to the singular point. The extraction auxiliary field for the displacements is defined as

$$\{u_E^{(i)}(r,\theta)\} = \begin{Bmatrix} u_{r,E}^{(i)} \\ u_{\theta,E}^{(i)} \end{Bmatrix} = r^{-\lambda_E}\{\Psi_E^{(i)}(\theta,-\lambda_E)\} \tag{20}$$

where the extraction eigenvalue is $\lambda_E = \lambda_j$ and the trigonometric functions $\{\Psi_E^{(i)}\}$ are the same as in Eq. (17). We choose $\lambda_E = \lambda_j$ to calculate the GSIF associated with the j-term, and hence, the exponent $-\lambda_E$ is negative. Note that the multiplicative

constant corresponding to the extraction field (analogous to the GSIF in the real field) is 1. Similarly, taking $\{\Phi_E^{(i)}\}$ as the same defined in Eq. (19), the stresses of the extraction field are defined as

$$\{\sigma_E^{(i)}(r,\theta)\} = \left\{ \begin{array}{c} \sigma_{rr,E}^{(i)} \\ \sigma_{\theta\theta,E}^{(i)} \\ \sigma_{r\theta,E}^{(i)} \end{array} \right\} = r^{-\lambda_E-1}\{\Phi_E^{(i)}(\theta,-\lambda_E)\} \tag{21}$$

Analogously, the traction vector of the extraction field is defined through the trigonometric functions $\{\Xi_E^{(i)}\}$ that result from the product $\sigma_{jk}n_j$ as

$$\{T_E^{(i)}(r,\theta)\} = r^{-\lambda_E-1}\{\Xi_E^{(i)}(\theta,-\lambda_E)\} \tag{22}$$

The trigonometric functions of the above definitions (20)–(22) depend on the eight parameters $a_E^{(i)}, b_E^{(i)}, c_E^{(i)}, d_E^{(i)}$, with $i = 1, 2$. The extraction field verifies the biharmonic Eq. (6) and, therefore, eight boundary conditions must be specified to calculate the coefficients.

The first four conditions are the same as in the original problem, i.e. the free boundaries must remain traction-free, see Eqs. (8). This is a necessary condition, as it has been used to show that the integral (3) is path-independent. The other four conditions are chosen so as to cancel the terms to be integrated along $\Gamma_C^{*(i)}$. These conditions are:

$$\begin{aligned} &u_\theta^{(1)}(r,0) - u_\theta^{(2)}(r,0) - f(u_r^{(1)}(r,0) - u_r^{(2)}(r,0)) = 0 \\ &\sigma_{r\theta}^{(1)}(r,0) = 0 \\ &\sigma_{r\theta}^{(2)}(r,0) = 0 \\ &\sigma_{\theta\theta}^{(2)}(r,0) - \sigma_{\theta\theta}^{(1)}(r,0) = 0 \end{aligned} \tag{23}$$

We can now apply the Mellin transform to the eight imposed conditions in an analogous manner to the preceding section. A new simultaneous system of eight equations is obtained:

$$\left[\begin{array}{cc} [B_{11}] & [B_{12}] \\ [B_{21}] & [B_{22}] \end{array} \right] \left\{ \begin{array}{c} v_E^{(1)} \\ v_E^{(2)} \end{array} \right\} = \left\{ \begin{array}{c} 0 \\ 0 \end{array} \right\} \tag{24}$$

where $v_E^{(i)} = (a_E^{(i)} b_E^{(i)} c_E^{(i)} d_E^{(i)})^{\mathrm{T}}$. The submatrices $[B_{ij}]$ are

$$[B_{11}] = [A_{11}] \tag{25}$$

$$[B_{12}] = [A_{12}] \tag{26}$$

$$[B_{21}] = \left[\begin{array}{cccc} -(\lambda+1) & 0 & -(1-\lambda) & 0 \\ 0 & 1 & 0 & 1 \\ 0 & 0 & 0 & 0 \\ -(\lambda+1) & f(\lambda+1) & (\lambda-1+m) & f(\lambda+1-m) \end{array} \right] \tag{27}$$

$$[B_{22}] = \left[\begin{array}{cccc} 0 & 0 & 0 & 0 \\ 0 & -1 & 0 & -1 \\ (\lambda+1) & 0 & (1-\lambda) & 0 \\ (\lambda+1) & -f(\lambda+1) & (1-\lambda-m) & f(m-\lambda-1) \end{array} \right] \tag{28}$$

and the characteristic equation of the auxiliary problem is obtained by making the determinant of the $[B]$ matrix equal to zero, yielding

$$\Delta_E(\lambda) = \cos(\lambda\pi)(\sin^2\lambda\psi - \lambda^2\sin^2\psi) + 0.5\sin(\lambda\pi)(\sin 2\lambda\psi + \lambda\sin 2\psi) + f\lambda(1-\lambda)\sin(\lambda\pi)\sin^2\psi = 0 \tag{29}$$

We have omitted a factor analogous to the one omitted in (15), since its roots have no physical meaning. It is straightforward to show that if λ is an eigenvalue of the original problem (15), then $-\lambda$ is an eigenvalue of the auxiliary problem used to define the extraction field (29). Thus, if we want to calculate the GSIF K_j^C associated with the eigenvalue λ_j, then $-\lambda_j = -\lambda_E$ is an eigenvalue of the auxiliary problem. An eigenvector problem is solved to find the eight parameters $a_E^{(i)}$, $b_E^{(i)}$, $c_E^{(i)}$, $d_E^{(i)}$ corresponding to $-\lambda_E$.

We now apply the path independent integral (3) to a circular path of radius ρ. Using the extraction field previously defined by (20) and (21), and the solution to the original problem given by (16) and (18), the following equation is obtained after algebraic manipulation:

$$I_{\Gamma_\rho}(u,u_E) = \sum_{j=1}^{\infty} \rho^{\lambda_j-\lambda_E} K_j^C C_{j,E} \tag{30}$$

In (30), we have taken into account that the integrals along $\Gamma_C^{*(i)}$ are zero due to the proper choice of the extraction field. Note that the integration path is circular ($\mathrm{d}s = \rho\mathrm{d}\theta$) and that the constant $C_{j,E}$ that relates the j-term with the extraction field E has been defined as

$$C_{j,E} = \int_{-\pi}^{\psi} (\lambda_j \{\Xi_j\}^{\mathrm{T}} \{\Psi_E\} + \lambda_E \{\Xi_E\}^{\mathrm{T}} \{\Psi_j\}) \mathrm{d}\theta \tag{31}$$

Since the integral (30) is path-independent, it does not depend on ρ. Therefore, for the rest of the modes j for which $\lambda_j \neq \lambda_E$, it must necessarily hold that $C_{j,E} = 0$. Only for the case in which j corresponds to the term to be extracted, i.e. $\lambda_j = \lambda_E$, it is verified that $C_{j,E} \neq 0$. This important property (orthogonality property) is used in the following section for the calculation of the GSIF K_j^C.

5. Equivalent domain integral for calculation of the GSIF

Let us define the exact fields solution of the original problem as u_{Ex}, σ_{Ex} (the corresponding traction vector is denoted as T_{Ex}). It is assumed that the exact fields can be expressed in the form (16) and (18). We are interested in obtaining K_j^C and, in accordance to Section 4, we define the extraction field for a value λ_E that equals the eigenvalue λ_j. Then, thanks to the orthogonality property, the Eq. (30) for a circular path reduces to:

$$I_{\Gamma_\rho}(u_{\mathrm{Ex}}, u_E) = K_j^C C_{j,E} \tag{32}$$

and therefore the GSIF K_j^C associated with the j-term can be computed through the expression:

$$K_j^C = \frac{1}{C_{j,E}} I_{\Gamma^*}(u_{\mathrm{Ex}}, u_E) = \frac{1}{C_{j,E}} \int_{\Gamma^*} (\{T_{\mathrm{Ex}}\}^{\mathrm{T}} \{u_E\} - \{T_E\}^{\mathrm{T}} \{u_{\mathrm{Ex}}\}) \mathrm{d}s \tag{33}$$

Note that I_{Γ_ρ} has been substituted by I_{Γ^*}, without loss of generality due to the path independency of the integral. Eq. (33) enables the computation of the GSIF through the contour integral I_{Γ^*}. We recall that Γ^* is an arbitrary path that starts at $\theta = -\pi$ and ends at $\theta = \psi$ (see Fig. 3).

We recast the contour integral I_{Γ^*} of (33) as a domain integral by adequately introducing a weight function and applying the divergence theorem. The approach is analogous to that used by Li et al. (1985) in the LEFM context for obtaining a domain integral equivalent to the J-contour integral proposed by Rice (1968). Since the traction vector is defined as $T_k = \sigma_{jk} n_j$ and using indicial notation, it is possible to rewrite I_{Γ^*} as

$$I_{\Gamma^*} = \int_{\Gamma^*} (\sigma_{jk}^{\mathrm{Ex}} u_k^E - \sigma_{jk}^E u_k^{\mathrm{Ex}}) n_j \mathrm{d}s \tag{34}$$

It is convenient to define the following contour integral I_P evaluated along a closed contour $P = P_0 + P_+ - \Gamma^* + P_-$ (see Fig. 4).

$$I_P = \int_P (\sigma_{jk}^{\mathrm{Ex}} u_k^E - \sigma_{jk}^E u_k^{\mathrm{Ex}}) q n_j \mathrm{d}s \tag{35}$$

Note that a function $q(x,y)$ has been introduced in the integrand. The so-called weight function q can be any sufficiently continuous scalar function defined within Ω^*, such that it vanishes on the outer contour P_0 and equals 1 on the inner contour Γ^*, i.e. it satisfies the following conditions:

$$q(x,y) = \begin{cases} 0 & \text{if}(x,y) \in \text{ domain outside } P_0 \\ 1 & \text{if}(x,y) \in \text{ domain inside } \Gamma^* \end{cases} \tag{36}$$

The q-function is a mathematical artifice that enables the conversion of the path independent integral (34) into a domain integral. As the free boundaries are traction-free (both for the exact and the extraction fields) and since the q-function vanishes along P_0, it holds that

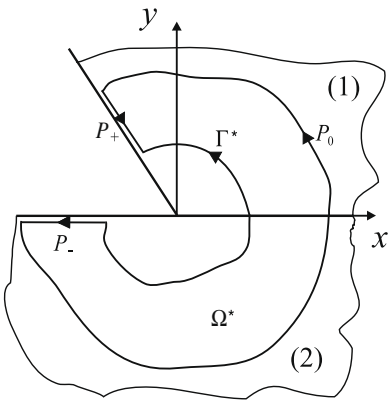

Fig. 4. Closed contour P used in the derivation of the equivalent domain integral.

$$I_P = -I_{\Gamma^*} \tag{37}$$

Invoking the divergence theorem, the contour integral I_P can be expressed as

$$I_P = \int_P (\sigma_{jk}^{\mathrm{Ex}} u_k^E - \sigma_{jk}^E u_k^{\mathrm{Ex}}) q n_j \mathrm{d}s = \int_{\Omega^*} \frac{\partial}{\partial x_j}[(\sigma_{jk}^{\mathrm{Ex}} u_k^E - \sigma_{jk}^E u_k^{\mathrm{Ex}}) q]\mathrm{d}\Omega \tag{38}$$

where Ω^* is the domain enclosed by P. The divergence of the integral can be expanded to give

$$I_P = \int_{\Omega^*} q\left(\frac{\partial \sigma_{jk}^{\mathrm{Ex}}}{\partial x_j} u_k^E - \frac{\partial \sigma_{jk}^E}{\partial x_j} u_k^{\mathrm{Ex}}\right)\mathrm{d}\Omega + \int_{\Omega^*} q\left(\sigma_{jk}^{\mathrm{Ex}} \frac{\partial u_k^E}{\partial x_j} - \sigma_{jk}^E \frac{\partial u_k^{\mathrm{Ex}}}{\partial x_j}\right)\mathrm{d}\Omega + \int_{\Omega^*} (\sigma_{jk}^{\mathrm{Ex}} u_k^E - \sigma_{jk}^E u_k^{\mathrm{Ex}}) \frac{\partial q}{\partial x_j}\mathrm{d}\Omega \tag{39}$$

The first of the integrals of (39) vanishes because both the exact and the extraction fields satisfy the equilibrium equation in the absence of body forces. In the second integral we can identify the exact and extraction strain fields, so (39) can be written as:

$$I_P = \int_{\Omega^*} q(\sigma_{jk}^{\mathrm{Ex}} \varepsilon_k^E - \sigma_{jk}^E \varepsilon_k^{\mathrm{Ex}})\mathrm{d}\Omega + \int_{\Omega^*} (\sigma_{jk}^{\mathrm{Ex}} u_k^E - \sigma_{jk}^E u_k^{\mathrm{Ex}}) \frac{\partial q}{\partial x_j}\mathrm{d}\Omega \tag{40}$$

Under a linear elastic behaviour is straightforward to show that $\sigma_{jk}^{\mathrm{Ex}} \varepsilon_k^E = \sigma_{jk}^E \varepsilon_k^{\mathrm{Ex}}$ due to the symmetry of the constitutive matrix and the first of the integrals in (40) cancels out. Therefore, taking into account the relationship (37), the sought equivalent domain integral (denoted as I_{Ω^*}) is obtained:

$$I_{\Gamma^*} = -\int_{\Omega^*} (\sigma_{jk}^{\mathrm{Ex}} u_k^E - \sigma_{jk}^E u_k^{\mathrm{Ex}}) \frac{\partial q}{\partial x_j}\mathrm{d}\Omega = I_{\Omega^*} \tag{41}$$

Finally, the following equation enables the computation of the GSIF through the domain integral:

$$K_j^C = \frac{I_{\Omega^*}}{C_{j,E}} = -\frac{1}{C_{j,E}} \int_{\Omega^*} (\sigma_{jk}^{\mathrm{Ex}} u_k^E - \sigma_{jk}^E u_k^{\mathrm{Ex}}) \frac{\partial q}{\partial x_j}\mathrm{d}\Omega \tag{42}$$

In practice, the analyst is usually interested in the computation of the GSIF associated with the first term of the asymptotic series expansion, i.e. $j = 1$, since the eigenvalue λ_1 produces the highest order of singularity. It is possible to compute any other GSIF K_j^C, as shown in the numerical examples.

When using a numerical method, such as the finite element method, to approximate the exact fields solution of the problem, the numerical calculation of the GSIF will be based on Eq. (33):

$$K_j^C = -\frac{1}{C_{j,E}} \int_{\Omega^*} (\sigma_{jk}^h u_k^E - \sigma_{jk}^E u_k^h) \frac{\partial q}{\partial x_j}\mathrm{d}\Omega \tag{43}$$

where the superscript $(\cdot)^h$ denotes an approximated numerical solution. To evaluate $\frac{\partial q}{\partial x_j}$ it is convenient to define q within each element as an interpolation from the corresponding nodal values:

$$q(x_1, x_2) = \sum_{n=1}^{nne} N_n(x_1, x_2) q_n \tag{44}$$

where nne is the number of nodes per element, N_n is the shape function associated with the node n and q_n is the nodal value of q at node n. The derivatives of q with respect to the spatial coordinates x_j are calculated as

$$\frac{\partial q}{\partial x_j} = \sum_{n=1}^{nne} \frac{\partial N_n(x_1, x_2)}{\partial x_j} q_n \tag{45}$$

The nodal values of q are conveniently defined between the inner contour Γ^* and the outer contour P_0. In this work we have used an annular distribution of the nodal values q_n, as described in Section 6.1.5. Since the derivative of q appears in the integrand of the domain integral (43), it is important that the derivative of q be continuous within each element in order to perform accurate numerical integrations. In principle, the analytical expression (42) is independent of the q-function, provided the above conditions regarding q are fulfilled. However, when implementing the procedure as a post-processing of a numerical solution, Eq. (43), there is a slight dependency on the chosen q-function due to the discretization error inherent, for example, in the FEM. The slight influence of the chosen q-function is caused by the FE solution which is not exact. If the FE solution were exact, there would be no influence of the chosen q-function.

As it happens with the contour integral I_{Γ^*}, the computation of the integrals through the FEM should avoid the elements close to the singular point, due to high discretization error. This is easily accomplished thanks to the domain independency of the integral. When implementing the method with the FEM, the domain integral is always more efficient and accurate than the contour integral. Moreover, it is more robust and easier to implement in a FE code because it is more consistent with the FE formulation.

6. Numerical verification

6.1. Problem 1

6.1.1. Finite element model

Fig. 5 shows the model analyzed with FE to verify the proposed domain integral. A linear elastic behaviour is assumed for both solids, with $E = 10^3$ [units of pressure], $\nu = 0.3$. The indenter angle is $\psi = 90^\circ$ and the friction coefficient is $f = 0.4$. This is a rather low value, and it has been chosen to reach a global sliding condition without applying large tangential forces to the indenter. The substrate dimensions are $t = 15$, $w = 40$ (consistent units of length for all dimensions), the contact width is $2a = 10$ and the height between the contact plane and the location where the loads are applied is $d = 10$. A plane strain condition is assumed with unit depth.

The load P is applied as a concentrated force at the middle of the indenter top. This force is evenly transferred to the top nodes of the indenter using multipoint constraints (MPCs), as if the top region were a rigid solid. The MPCs enforce that the degrees of freedom (DOFs) on the indenter top nodes are tied and equal to the DOFs of the node where the load is applied. In addition, the rotational DOF of the indenter top is constrained. The global sliding condition is attained through two load steps. In the first load step, P is increased to the maximum value of $P_{\max} = 100$. During the second load step, P is kept at $P_{\max}$ and simultaneously a forced displacement U to the left is prescribed, with a maximum value of $\Delta U|_{\max} = 10$ [units of length] (i.e. $|\Delta U|_{\max} = 2a$). The prescribed displacement to the left controls the implicit tangential loads and guarantees the numerical convergence of the analysis once the global sliding condition is reached. All results for Problem 1 are referred to the instant in which the prescribed displacement to the left is $|\Delta U|/a = 0.004$. At this time instant, the global sliding condition is already reached.

Two FE meshes have been used (coarse and refined) as shown in Fig. 6. In addition, the coarse mesh was analyzed with both linear 4-node elements and quadratic 8-node elements. The refined mesh was only analyzed with quadratic 8-node elements. For the coarse mesh, the element size next to the singular corner is $0.05a$. For the refined mesh, the element size is $\approx 4 \times 10^{-3} a$. The analyses were carried out with the FE code ABAQUS™.

6.1.2. Singularity order

In order to obtain the eigenvalue associated with the left corner singularity, the root in the interval $]0,1[$ of the characteristic Eq. (15) must be found. The indenter slides to the left, so the friction coefficient must be defined with negative sign, $f = -0.4$ (Comninou, 1976). The first eigenvalue obtained in the interval $]0,1[$ is $\lambda_1 = 0.59832$. For the eigenvalue associated with the right corner sliding to the left, the friction coefficient is taken as $f = +0.4$. In this latter case, it is verified that the characteristic equation has no real roots in the interval $]0,1[$ and therefore the stress field is non singular. The objective is to calculate K_1^C associated with $\lambda_1 = 0.59832$ in order to fully characterize the singular field in the vicinity of the left corner.

Given that this problem has no known reference solution, the effectivity of the proposed domain integral is assessed by comparison with the GSIF calculations via stress extrapolation and the contour integral method.

6.1.3. GSIF calculation via stress extrapolation

The stress extrapolation was carried out by collocation of the $\sigma_{\theta\theta}$ stress field along the contact plane $\theta = 0$ in a region sufficiently close to the left corner. Taking the limit $r \to 0$ of (18) and solving for K_1^C:

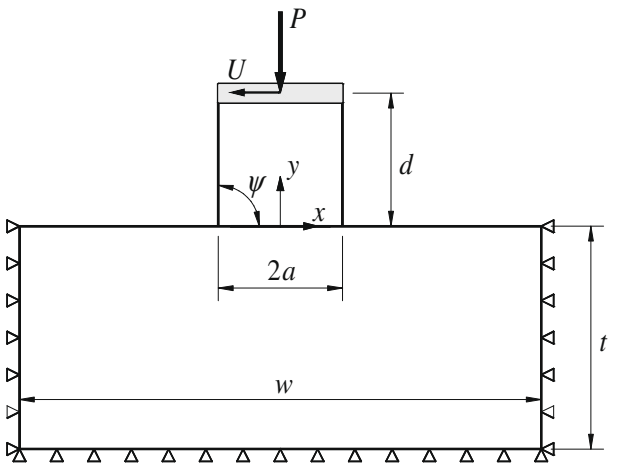

Fig. 5. Problem 1: Model of the complete contact problem (substrate and indenter).

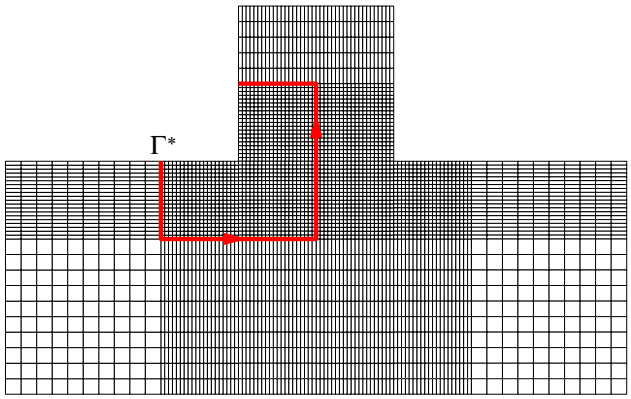

(a) Coarse mesh: analyzed both with linear and quadratic elements.

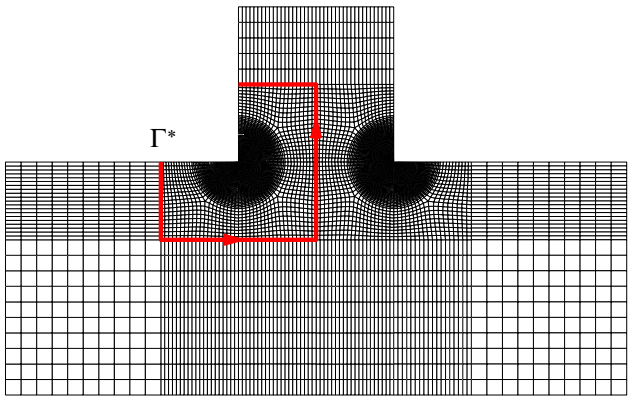

(b) Refined mesh: analyzed only with quadratic elements.

Fig. 6. Problem 1: Two discretizations used in the FE analyses. Note the location of the path Γ^* used for the contour integral evaluation.

$$K_1^C = \lim_{r\to 0} \frac{\sigma_{\theta\theta}(r,0)}{r^{\lambda_1-1}\Phi^{(i)}_{\theta\theta,1}(0)} \tag{46}$$

for any of the solids (i), since the stress component $\sigma_{\theta\theta}$ is continuous across the contact plane $\theta = 0$. To improve the quality of the FE stresses $\sigma_{\theta\theta}(r,0)$ on the contact plane, they were calculated by extrapolation to nodes from the integration points and subsequent nodal averaging. It is easier to apply (46) to the indenter, i.e. solid (1). The trigonometric function in (46) is $\Phi^{(1)}_{\theta\theta,1}(0) = 1.44065$ and the extracted GSIFs are shown in Table 1. For coarse meshes, it is difficult to establish the singular dominated region and correlations are non-repetitive. As expected, the stress extrapolation technique yields good estimations of K_1^C for refined meshes around the singular point. Note that the dimension of K_1^C is [units of pressure] × [units of length]$^{1-\lambda_1}$.

6.1.4. GSIF calculation via the path independent contour integral

Fig. 6 shows the paths Γ^* along which the path independent contour integral was evaluated using (33). For this calculation, we used the nodal values of the FE displacement solution and the nodal averaged stresses extrapolated from the integration points. The contour integral was performed using three Gauss integration points along each of the element sides traversed by the path Γ^*. It was checked that a higher order integration yielded virtually the same results. The constant

Table 1
Calculation of K_1^C using the stress extrapolation technique, the contour integral along Γ^* and the domain integral with the q-function shown in Fig. 7.

Mesh	Elements	K_1^C (stress extrap.)	K_1^C (contour integral)	K_1^C (domain integral)
Coarse	Linear	−11.225	−10.370	−10.741
Coarse	Quadratic	−10.524	−10.738	−10.731
Refined	Quadratic	−10.708	−10.722	−10.715

[Units of K_1^C] = [units of pressure] × [units of length]$^{1-\lambda_1}$.

$C_{1,E}$ needed in (33) was calculated according to its definition (31), resulting $C_{1,E} = -0.010358$ ($C_{j,E}$ is a dimensionless magnitude). The results for K_1^C using the contour integral are shown in Table 1. In (Fuenmayor et al., 2005) a more detailed analysis of the contour integral performance is presented: the path independency is verified calculating results for different paths, the effect of large sliding conditions ΔU is considered and other models with different indenter angles ψ are studied.

6.1.5. GSIF calculation via the proposed domain integral

In order to calculate the GSIF using the domain integral (42), the q-function must be defined in accordance with the requirements presented in Section 5. For Problem 1, an annular q-function was defined, with a linear distribution between an inner radius $R_{min}/a = 0.4$ and an outer radius $R_{max}/a = 1$. In addition, $q = 1$ for all nodes enclosed by R_{min} and $q = 0$ for all nodes outside R_{max}. Fig. 7 shows the q-function used in the calculation of the GSIFs presented in Table 1. Note that the extraction field used in (42) depends on the solid where the integration is performed, as for the contour integral method.

As expected, the results of Table 1 for the domain integral method tend to be more independent of the mesh and type of element than for the other methods, proving that this technique is robust and efficient. Note that using a coarse mesh with linear elements, the first three significative digits coincide with the result for the refined quadratic mesh. On the other hand, it can be observed that the use of the contour integral method with the linear coarse mesh reduces the accuracy to only two significative digits. Of course, the application of the stress extrapolation technique to a coarse linear mesh is not recommended.

The q-function enables to control the integration domain. In this way, the integration over elements next to the singular point, where the discretization error is the highest, can be avoided. Due to the high error in the elements next to the singular point, it was proved that the result was affected by the inclusion of these elements within the integration domain. However, if these elements are not included, it was verified by changing R_{min} and R_{max} that the results are virtually the same and in practice domain independent. The results would be absolutely domain independent if the FE solution were exact. Table 2 shows the influence of the integration region, i.e. the influence of the q-function, for the coarse linear mesh. The element size next to the singular corner is denoted by h_{sing}. It can be seen that if $R_{min} < h_{sing}$, the estimation of K_1^C is not accurate. Therefore, it is recommended to use a q-function such that $R_{min} \gtrapprox 2h_{sing}$. The results show that the calculation of K_1^C is not sensitive to the integration region if this is far enough from the singular corner.

6.2. Problem 2

6.2.1. Model description

The previous example has no known reference solution, so it is difficult to assess the accuracy of the proposed method. To further test the precision of the calculated GSIFs, we have set a finite domain problem, see Fig. 8, whose boundary conditions correspond to the exact tractions and displacements of the analytical asymptotic fields given by Eqs. (16) and (18). Three terms of the asymptotic series have been taken, $j = 1 - 3$, so as to model the superposition of three modes of the series expansion. The equivalent exact tractions for the first three modes have been imposed on the boundaries of the two solids (Neumann boundary conditions, BCs), respecting the two traction-free sides and with the exception of the contacting sides. For the contacting boundaries, exact displacements have been prescribed in a weak form (Dirichlet BCs). This is equivalent to solving two separate linear elastic singular problems, because the contact interaction is substituted by exact Dirichlet BCs.

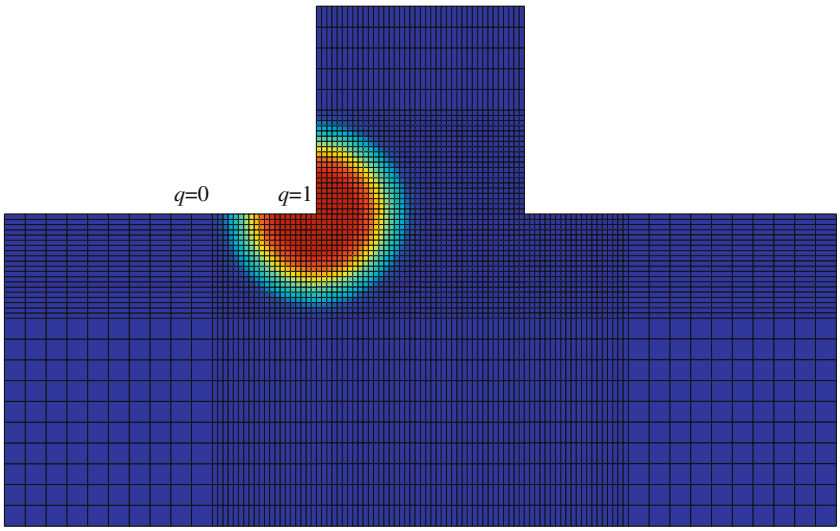

Fig. 7. q-Function used in the domain integral (42). The distribution of q is annular, with a linear variation between $R_{min}/a = 0.4$ and $R_{max}/a = 1$.

Table 2
Calculation of K_1^C using the domain integral with several annular q-functions.

$\frac{R_{min}}{h_{sing}}$	K_1^C $\frac{R_{max}}{h_{sing}} = 8$	K_1^C $\frac{R_{max}}{h_{sing}} = 20$
0.0	−14.459	−12.229
0.2	−14.073	−12.054
0.4	−13.666	−11.875
2	−10.849	−10.777
4	−10.789	−10.753
6	−10.763	−10.745
8	–	−10.741
10	–	−10.740
12	–	−10.740
14	–	−10.740
16	–	−10.740

R_{min} is varied for two different R_{max}. Coarse linear mesh.
[Units of K_1^C] = [units of pressure] × [units of length]$^{1-\lambda_1}$.

The indenter angle ψ is 90° and the value of the friction coefficient is $f = -1.6$ indicating a friction sliding to the left (leading corner). The eigenvalues of the applied terms of the series expansion are the first three positive roots of (15): $\lambda_1 = 0.17944$, $\lambda_2 = 1.88010$ and $\lambda_3 = 2.87501$. Note that only the first of these eigenvalues leads to a singular stress field. In fact, the relatively high value of the friction coefficient and the corresponding small value of λ_1 lead to a strong singular stress field, which is much stronger than, for example, the singularity in LEFM ($\sigma \propto r^{0.5-1}$). The material is assumed to have a linear elastic behaviour, with $E = 210,000$ [units of pressure] and $\nu = 0.3$. In generating the boundary conditions, we have assumed the following multiplier constants (GSIFs): $K_{1,ex}^C = 1.0$, $K_{2,\ ex}^C = -7.0 \times 10^{-4}$ and $K_{3,ex}^C = 11.0 \cdot 10^{-6}$ with dimensions [units of pressure] × [units of length]$^{1-\lambda_j}$. These are the exact reference solutions for the subsequent analyses.

In this problem, a different definition of the q-function has been introduced that depends on a single parameter R_q. Instead of using R_{min} and R_{max} as in Problem 1, we define a single radius R_q (see Fig. 8) to simplify the study of the q influence. The definition is as follows: all nodes within a circle of radius R_q centered at the singular point take the value of 1 and $q = 0$ at the rest of nodes. The q-function is then defined as a bilinear finite element interpolation within the nodal values of q. Therefore, only elements traversed by the circumference R_q have a non-zero gradient of q and contribute to the domain integral in (42).

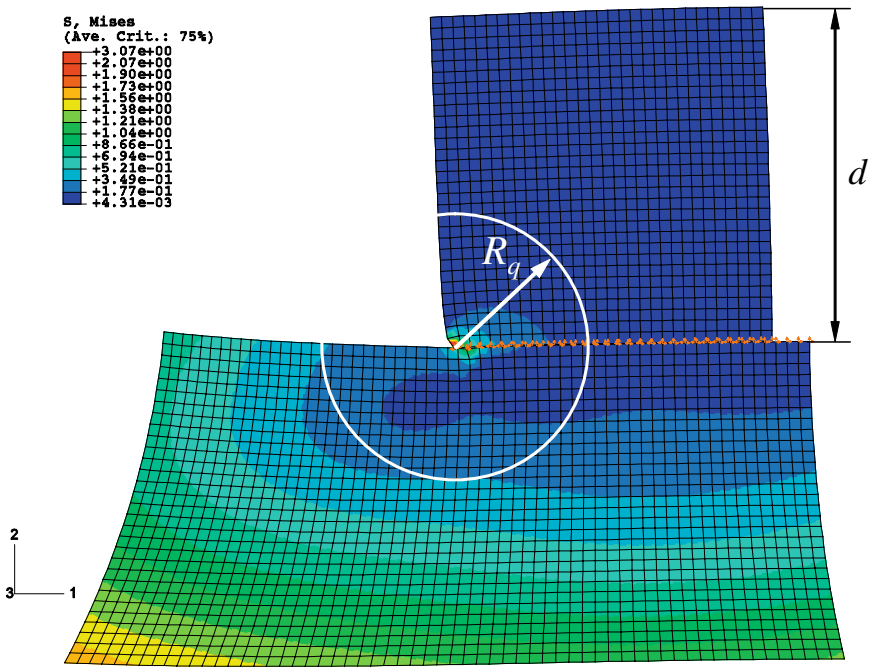

Fig. 8. Finite domain of the analytical sliding contact problem. Deformed shape of the von Mises plot for the third mesh of the sequence. The boundary conditions correspond to the three first terms of the analytical asymptotic field. R_q is the radius of the q-function used to evaluate the domain integral.

6.2.2. Calculation of the GSIFs K_j^C

A sequence of six uniformly refined meshes (linear elements) has been analyzed to verify the accuracy of the proposed domain integral method. The ratios of the element size h to the height d of the indenter are 1/9, 1/15, 1/30, 1/45, 1/60 and 1/90. The mesh shown in Fig. 8 corresponds to mesh number 3. For each mesh, the domain integral has been applied with fourteen different ratios of R_q/d, d being the indenter height.

Fig. 9 shows the calculations for the GSIFs K_1^C, K_2^C and K_3^C scaled with respect to their exact solutions for three of the meshes and for different R_q. In general, it can be seen that the error when computing the singular mode GSIF K_1^C is the largest. This is due to the reduced ability of the FE uniform meshes to represent such a singular field. On the contrary, the extraction of K_3^C is fairly accurate with slightly overestimating results in this case.

As in Problem 1, Fig. 9 also shows that the method tends to be domain-independent (i.e. independent of the q-function) provided R_q is sufficiently large, avoiding integration over the elements next to the singularity. When R_q traverses these elements (e.g. low R_q with coarse meshes as in mesh 2), results are not accurate. This is specially evident for K_3^C, because the singular term dominates in the zone close to the singular point and the smooth field corresponding to the third mode is not captured by the FE approximation.

The relative percentage error in $K_j^C, j = 1-3$ for the six meshes of the sequence is plotted in Fig. 10. An intermediate value of R_q was taken for the calculations, $R_q/d = 0.533$. Again, it is shown that K_1^C is computed with a larger error than K_2^C and K_3^C for all the meshes. Note that the absolute value of the error in K_3^C is plotted due to the overestimating results for K_3^C. The convergence rate for the singular GSIF K_1^C is about 0.64 and a similar trend is observed for the other GSIFs. The uniformly refined meshes do not remove the effect of the singularity (as opposed to h-adapted meshes, i.e. meshes that have elements of different sizes to conform to the singularity). As a consequence, and since the order of the singularity is high, the convergence rate is rather low. As a comparative value, the *a priori* SIF convergence rate in a LEFM problem for a sequence of uniformly refined meshes with linear elements would be 1 (Giner et al., 2004).

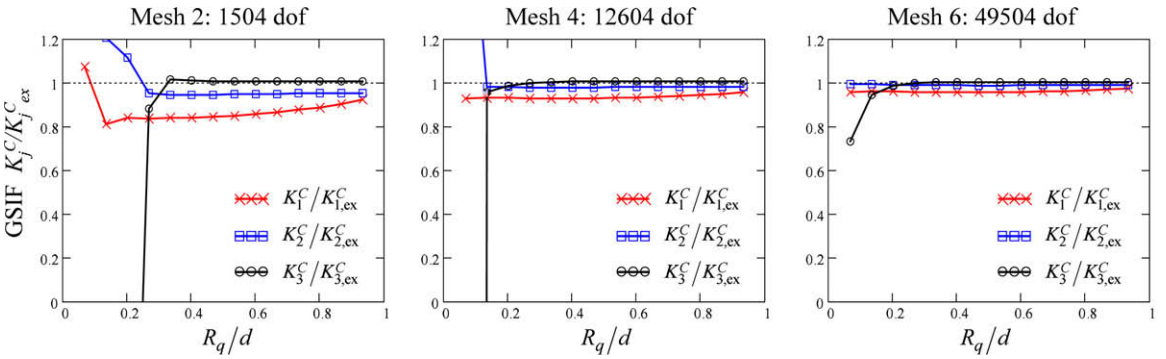

Fig. 9. GSIF calculations for the first three modes, $K_j^C, j = 1-3$, for meshes 2, 4 and 6. The results are computed for fourteen different q-functions, defined by varying R_q. d is the indenter height, see Fig. 8.

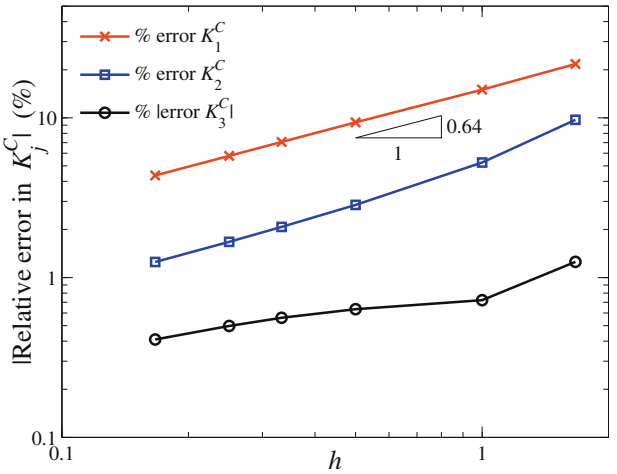

Fig. 10. Relative percentage error in and estimated convergence rate for the six meshes of the sequence. The q-function was defined by $R_q/d = 0.533$.

7. Conclusions

In this study, a new domain integral has been proposed for the extraction of the generalized stress intensity factor (GSIF) in sliding complete contacts. The integral is based on an energetic approach (Betti's reciprocal theorem) and is derived from a path independent contour integral. The application of these integrals involves the use of a conveniently defined extraction field. For the domain integral, it is also necessary to define a q-function (analogous to the q-function used for domain integrals in the LEFM context) that controls the integration domain of the method.

By means of numerical examples, it has been verified that the domain integral method is accurate and efficient, provided the elements next to the singular point are not included in the integration domain. The proposed technique is general and is very well suited to the post-processing of a numerical solution obtained by the FEM. Moreover, the domain integral is always more accurate and efficient than the contour integral and the implementation within a FE code is much more straightforward. The method also enables to extract the multiplier constants associated with other eigenvalues of the series expansion. The results show that the accuracy of the domain integral is good even with coarse linear discretizations. This makes possible to use discretizations of low computational-cost without affecting the GSIF estimation, which is very convenient for the modelling of non-linear contact problems.

Acknowledgements

The authors thank Ministerio de Ciencia y Tecnología for the support received in the framework of the project DPI2007-66995-C03-02. The financial support received from Vicerrectorado de Investigación, Desarrollo e Innovación (Universidad Politécnica de Valencia) and Conselleria d'Empresa, Universitat i Ciència (Generalitat Valenciana) is also gratefully acknowledged.

References

Banks-Sills, L., 1991. Application of the finite element method to linear elastic fracture mechanics. Applied Mechanics Reviews 44, 447–461.
Barber, J.R., 2002. Elasticity. Kluwer Academic Publishers, Dordrecht.
Comninou, M., 1976. Stress singularity at a sharp edge in contact problems with friction. Journal of Applied Mathematics and Physics (ZAMP) 27, 493–499.
deLorenzi, H.G., 1985. Energy release rate calculations by the finite element method. Engineering Fracture Mechanics 21 (1), 129–143.
Fuenmayor, F.J., Giner, E., Tur, M., 2005. Extraction of the generalized stress intensity factor in gross sliding complete contacts using a path-independent integral. Fatigue and Fracture of Engineering Materials and Structures 28, 1071–1085.
Gdoutos, E.E., Theocaris, P.S., 1975. Stress concentration at the apex of a plane indenter acting on an elastic half-plane. Journal of Applied Mechanics 42, 688–692.
Giner, E., Fuenmayor, F.J., Tarancón, J.E., 2004. An improvement of the EDI method in linear elastic fracture mechanics by means of an *a posteriori* error estimator in *G*. International Journal for Numerical Methods in Engineering 59, 533–558.
Gosz, M., Moran, B., 2002. An interaction energy integral method for computation of mixed-mode stress intensity factors along non-planar crack fronts in three dimensions. Engineering Fracture Mechanics 69, 299–319.
Hattori, T., Sakata, S., Watanabe. T., 1988. A stress singularity parameter approach for evaluating adhesive and fretting strength. ASME Book No. G00485, MD-Vol. 6, p. 43.
Hattori, T., 1994. Fretting fatigue problems in structural design. In: Waterhouse, R.B., Lindley, T.C. (Eds.), Fretting Fatigue. ESIS 18. Mechanical Engineering Publications, London, pp. 437–451.
Hattori, T., Nakamura, M., Watanabe, T., 2003. Simulation of fretting-fatigue life by using stress-singularity parameters and fracture mechanics. Tribology International 36 (2), 87–97.
Lazzarin, P., Zambardi, R., 2001. A finite-volume-energy based approach to predict the static and fatigue behavior of components with sharp V-shaped notches. International Journal of Fracture 112, 275–298.
Lazzarin, P., Berto, F., Gómez, F.J., Zappalorto, M., 2008. Some advantages derived from the use of the strain energy density over a control volume in fatigue strength assessments of welded joints. International Journal of Fatigue 30, 1345–1357.
Li, F.Z., Shih, C.F., Needleman, A., 1985. A comparison of methods for calculating energy release rates. Engineering Fracture Mechanics 21 (2), 405–421.
Mugadu, A., Hills, D.A., 2002. A generalised stress intensity approach to characterising the process zone in complete fretting contacts. International Journal of Solids and Structures 39, 1327–1335.
Mugadu, A., Hills, D.A., Limmer, L., 2002. An asymptotic approach to crack initiation in fretting fatigue of complete contacts. Journal of the Mechanics and Physics of Solids 50 (3), 531–547.
Omer, N., Yosibash, Z., 2005. On the path independency of the point-wise *J* integral in three-dimensions. International Journal of Fracture 136, 1–36.
Rice, J.R., 1968. A path independent integral and the approximate analysis of strain concentration by notches and cracks. Journal of Applied Mechanics 35, 379–386.
Stern, M., Becker, E.B., Dunham, R.S., 1976. A contour integral computation of mixed-mode stress intensity factors. International Journal of Fracture 12 (2), 359–368.
Szabó, B.A., Babuška, I., 1991. Finite Element Analysis. John Wiley & Sons Inc., New York.
Tur, M., Mugadu, A., Fuenmayor, F.J., Hills, D.A., 2002a. On the analysis of singular stress fields. Part 1: finite element formulation and application to notches. Journal of Strain Analysis for Engineering Design 37 (5), 437–444.
Tur, M., Fuenmayor, F.J., Mugadu, A., Hills, D.A., 2002b. On the analysis of singular stress fields. Part 2: application to complete slipping contacts. Journal of Strain Analysis for Engineering Design 38 (3), 207–217.
Tur, M., Giner, E., Fuenmayor, F.J., 2006. A contour integral method to compute the generalized stress intensity factor in complete contact under sliding conditions. Tribology International 39, 1074–1083.
Williams, M.L., 1952. Stress singularities resulting from various boundary conditions in angular corners of plates in extension. Journal of Applied Mechanics 19, 526–528.
Yosibash, Z., Omer, N., 2007. Numerical methods for extracting edge stress intensity functions in anisotropic three-dimensional domains. Computer Methods in Applied Mechanics and Engineering 196, 3624–3649.